

Benefits of a High Performance Airborne Gravity Gradiometer for Resource Exploration

Annechione, M. A. ^[1], Moody, M. V. ^[2], Carroll, K. A. ^[1], Dickson, D. B. ^[3], Main, B. W. ^[1]

1. Gedex Inc., Mississauga, Ontario, Canada
2. Department of Physics, University of Maryland, College Park, Maryland
3. DeBeers Canada, Toronto, Ontario, Canada

ABSTRACT

Gedex Inc and the University of Maryland are developing a high performance airborne superconducting gravity gradiometer system (HD-AGG). Preliminary laboratory test data demonstrating the low noise floor of the instrument are presented. The benefits of a low noise floor for resource exploration are demonstrated. The single-axis prototype provides measurements of one gravity gradient tensor diagonal element combination. The complete 3-axis system will provide measurements of three gravity gradient tensor diagonal element combinations. The gravity gradiometer will be housed in a liquid helium cryostat to maintain superconducting temperatures which will in turn be placed on a six-degree-of-freedom motion isolation platform. Instrument design inherently rejects translational accelerations and the isolation system is designed to isolate the sensor from rotational and translational vibrations. Preliminary laboratory tests demonstrating the gradiometer data to have a noise PSD below $1Eo/\sqrt{Hz}$ from 0.05 to 1 Hz are promising. The target noise floor for the instrument in airborne mode is $1Eo/\sqrt{Hz}$ from 0.001 to 1 Hz. The benefits of such high accuracy, high spatial resolution data for resource exploration are demonstrated by computing the vertical gradient of the vertical gravity component response of a kimberlite model, and by adding expected noise to the response. An airborne gravity gradiometer having the stated performance is capable of imaging deposits beyond the detection capability of and with greater resolution than current operational, non-superconducting technology.

INTRODUCTION

The gravity gradient tensor of the Earth is given by:

$$\mathbf{\Gamma} = \begin{bmatrix} \Gamma_{xx} & \Gamma_{xy} & \Gamma_{xz} \\ \Gamma_{yx} & \Gamma_{yy} & \Gamma_{yz} \\ \Gamma_{zx} & \Gamma_{zy} & \Gamma_{zz} \end{bmatrix} = \begin{bmatrix} \frac{\partial g_x}{\partial x} & \frac{\partial g_x}{\partial y} & \frac{\partial g_x}{\partial z} \\ \frac{\partial g_y}{\partial x} & \frac{\partial g_y}{\partial y} & \frac{\partial g_y}{\partial z} \\ \frac{\partial g_z}{\partial x} & \frac{\partial g_z}{\partial y} & \frac{\partial g_z}{\partial z} \end{bmatrix}$$

where (g_x, g_y, g_z) is the Earth's gravity vector. Gravity potential satisfies Laplace's equation:

$$\Gamma_{xx} + \Gamma_{yy} + \Gamma_{zz} = 0 \quad (1)$$

and the gradient tensor is symmetric: $\Gamma_{ij} = \Gamma_{ji}$ for $i \neq j$. The vertical gravity component, g_z , and its vertical gradient, Γ_{zz} , are most amenable to qualitative interpretation because local

maxima and minima identify the (x,y) locations of compact anomalous masses within homogeneous media. The local minima/maxima and zeros of the horizontal gravity components, g_x and g_y , and the remaining gradient tensor elements locate and identify other features of compact anomalous mass distributions within homogeneous media; for example, the edges, corners and strikes of sources. The gradient Γ_{xx} is preferred over vertical gravity because g_x is inherently a more laterally diffuse image of the density distribution compared to Γ_{xx} (Li, 2001). For example, Figure 1 shows the vertical gravity profile and the vertical gradient of vertical gravity profile over a 100 m thick contact having a density contrast of 0.5 g/cc, 250 m above its center. The gravity gradient fields offer enhanced shorter wavelength information and are better at imaging shallower sources than the gravity vector components. From the measurement perspective, gravity gradiometers are inherently (to a first order) insensitive to translational accelerations whereas gravimeters sense translational accelerations which must be observed by independent non-inertial means (i.e. GPS kinematic accelerations).

Current, operational, non-superconducting airborne gravity gradiometers (AGG) provide gravity gradient maps having reported estimated noise levels ranging between 3 Eo RMS at

150 m wavelength resolution (Boggs et al., 2007) and 15 Eo RMS at wavelengths from 400 to 600 m (Murphy et al., 2007). The latter performance level places limits on the detectability and gravity gradient imaging capabilities of economic kimberlites, ore deposits and other geological structures of interest in resource exploration. The former performance level is difficult to achieve systematically because motion induced errors are present. A gravity gradiometer system having a noise floor of 1 Eo RMS over wavelengths of tens of meters to tens of kilometers in airborne mode, is sought to assist resource exploration activities.

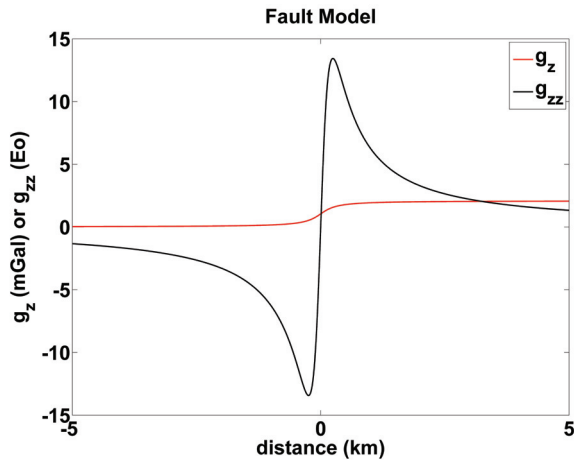


Figure 1: Vertical gravity and vertical gradient of vertical gravity over a 100 m thick contact having a density contrast of 0.5 g/cc, 250 m above its center.

METHOD

Sensor Design

In order to produce a gravity gradient map with a final accuracy of 1 Eo RMS at a wavelength resolution of 50 m from gravity gradiometer data acquired in an airborne environment, it is necessary to begin with a gravity gradiometer having the lowest possible intrinsic noise and the highest possible material and circuit stability. This is achieved with superconducting mechanical components, sensing coils and SQUID amplifiers. Material and circuit stability allows precise scale factor matching and accurate rejection of dynamic errors.

Gedex Inc is developing an airborne gravity gradiometer system (HD-AGG) using a superconducting gravity gradiometer developed by the University of Maryland (Moody and Paik, 2004). The HD-AGG will incorporate a six-degree-of-freedom motion isolation sub-system (GeoMIM) designed to reduce errors associated with the down-conversion of high-frequency platform jitter outside the signal band to lower frequencies within the signal band via non-linear acceleration terms in the dynamic characterization model.

The single-axis gravity gradiometer prototype uses a pair of matched angular accelerometers and provides measurements of the gravity gradient tensor diagonal element combination $\Gamma_{xx}-\Gamma_{yy}$ or the off-diagonal element Γ_{xy} depending on the mounting orientation of the pair of angular accelerometers. The full three-

axis sensor (Figure 2) will provide observations of $\Gamma_{xx}-\Gamma_{yy}$ (or Γ_{xy}), $\Gamma_{xx}-\Gamma_{zz}$ and $\Gamma_{yy}-\Gamma_{zz}$. Single-axis gravity gradiometer data can be transformed into Γ_{zz} using Fourier domain techniques (Mickus and Hinojosa, 2001) while Γ_{xx} , Γ_{yy} and Γ_{zz} are obtained from the 3-axis sensor by simple linear combinations of the observations and by invoking Laplace's equation (Eqn. 1).

Intrinsic (Brownian and SQUID amplifier) noise is $\sqrt{0.0002}$ Eo/ $\sqrt{\text{Hz}}$ at 0.5 Hz and $\sqrt{0.002}$ Eo/ $\sqrt{\text{Hz}}$ at 5 mHz, well below the target accuracy of the HD-AGG. Temperature and dynamics-related noise sources are being characterized in the laboratory. MicroKelvin-level temperature control is required to compensate for gradiometer thermal drift at the 1 Eo level. This requires careful design of the cryostat and control electronics. The gradiometer sensing current ratios are adjusted to compensate for angular accelerometer imbalances. Angular accelerometer center-of-mass offsets and axis misalignments are measured and used in an error compensation formula with auxiliary translational and angular accelerometer data. The quadratic response coefficients of the gradiometer are also measured and employed for error compensation.

In addition to system-specific errors, the sum of self-gradient correction errors and terrain correction errors must be less than the stated target accuracy. The self-gradient correction compensates for the gradiometer signal resulting from the displacements of the gradiometer with respect to the aircraft and the equipment and crew surrounding the gradiometer. The terrain correction subtracts the gradient signal of the terrain mass from the gradient data. This signal dominates the gradient signal from the underlying geology in areas of moderate topographic relief.

Continuing work is under way on refining the dynamics-related correction model parameters. At the time of going to press, the SQUID amplifier and temperature sensing circuitries, the motion isolation subsystem and the cryostat subsystem were being assembled. The self-gradient correction problem was being addressed and terrain correction software was being licensed.

Gravity Gradient Forward Modelling

An arbitrary density distribution within a half-space volume of the ground may be modelled as an assemblage of 3D prismatic cells each having uniform density. The gravity gradient observed at a point above the volume is obtained by summing the gradient responses of each cell at the observation point. The Colorado School of Mines forward modelling program implements this approach (Gravity and Magnetics Research Consortium, 2003). The gravity gradient Γ_{ij} at a point \mathbf{r}_0 is computed using:

$$\Gamma_{ij}(\mathbf{r}_0) = \gamma \sum_{k=1}^M \rho_k \left\{ \int_{\Delta V_k} \frac{\partial}{\partial x_i} \frac{\partial}{\partial x_j} \frac{1}{|\mathbf{r} - \mathbf{r}_0|} dv \right\}$$

where γ is the gravitational constant, ρ_k is the density of the k -th cell, ΔV_k is the volume of the k -th cell, M is the total number of cells, and \mathbf{r} is a point within the k -th cell. The integral in

parentheses is the gradient response at r_0 of the k-th cell having unit density.

The gravity gradients are computed along simulated survey traverse and control lines of given spacing assuming a data sampling rate of 2 Hz and an aircraft speed of 51 m/s (100 knots). Time sequences of normally distributed random noise of standard deviation 1 Eo and 7 Eo are added to the computed values. The simulated flight line data are then gridded to produce gravity gradient maps with different noise levels.

Alternatively, the gravity gradients may be computed on regular 2D grids and 2D grids of noise equivalent to 1 Eo/ $\sqrt{\text{Hz}}$ and 7 Eo/ $\sqrt{\text{Hz}}$, given the grid node spacing and an assumed aircraft speed, may be added to the noise-free gradient grids. The time sequences of noise and the 2D noise grids are generated in Matlab®.

The lowest noise level of gravity gradient data from current operational non-superconducting AGGs reported in the geophysics literature is 1.4 Eo within a 0.18 Hz bandwidth (Boggs et al., 2005). This noise level corresponds to a flat power spectral density (PSD) of 3.3 Eo/ $\sqrt{\text{Hz}}$ assuming an aircraft speed of 100 knots. Industry regards this as exceptional results, likely the consequence of exceptionally low turbulence. A noise level of 15 Eo/ $\sqrt{\text{Hz}}$ (Murphy et al., 2007) would represent more typical data. A flat noise PSD of 7 Eo/ $\sqrt{\text{Hz}}$ from 0.001 Hz to 1 Hz is used here to represent optimistic results for non-superconducting operational AGGs operated under typical survey conditions. A flat noise PSD of 1 Eo/ $\sqrt{\text{Hz}}$ from 0.001 Hz to 1 Hz is the HD-AGG target (systematic) performance under typical survey conditions.

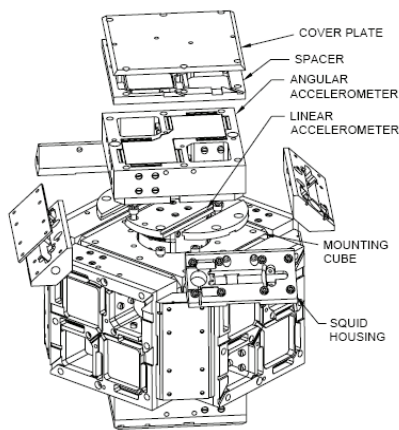


Figure 2: Full 3-axis gravity gradiometer design (Moody and Paik, 2004).

Table 1: Two-kimberlite model parameters.

	Thickness (m)	Density (g/cc)	Radius (m)	
			0.79 Ha	3.1 Ha
overburden	50	2.0	NA	NA
crater	200	2.25	50	100
diatreme	200	2.5	25	50
host	NA	2.6	NA	NA

RESULTS

Sensor Design

Figure 3 shows preliminary gradiometer data from a quiescent laboratory test conducted at the University of Maryland on December 5, 2006. The signal was acquired over a period of about 30 minutes. Only seismic noise was present. Dynamics-related corrections were applied. A temperature correction was applied using temperature data obtained with off-the-shelf electronics providing temperature control of +/- 20 microKelvin. The residual gradient error standard deviation is less than 0.76 Eo. The square root of the PSD is less than 1 Eo/ $\sqrt{\text{Hz}}$ from about 0.05 Hz to 1 Hz.

These results are promising for several reasons. First, the gradiometer was not housed in the GeoMIM. Down-conversion of high-frequency platform jitter from seismic noise is present. Second, custom temperature control electronics, allowing microKelvin-level temperature control, was not being used. This resulted in temperature variations which could not be entirely compensated.

Gravity Gradient Forward Modelling

Kimberlites are pipe-like geological structures which are a source of mined diamonds. The surface area of kimberlites ranges from 0.5 to 150 Ha. Kimberlite size is not indicative of diamond content, so that smaller kimberlites may be very economic.

Figure 3 shows a two kimberlite model; one kimberlite having a diameter of 200 m (3.1 Ha), the other a diameter of 100 m (0.79 Ha). Table 1 lists the model parameters. Figure 4 shows the Γ_{xx} responses with 1 Eo/ $\sqrt{\text{Hz}}$ and 7 Eo/ $\sqrt{\text{Hz}}$ noise added to the simulated flight line data. The 1 Eo/ $\sqrt{\text{Hz}}$ data reveals coherent signal at the location of the 0.79 Ha kimberlite and clearly images the 3.1 Ha kimberlite. The 7 Eo/ $\sqrt{\text{Hz}}$ data shows no coherent signal at the location of the 0.79 Ha kimberlite and poorly images the 3.1 Ha kimberlite.

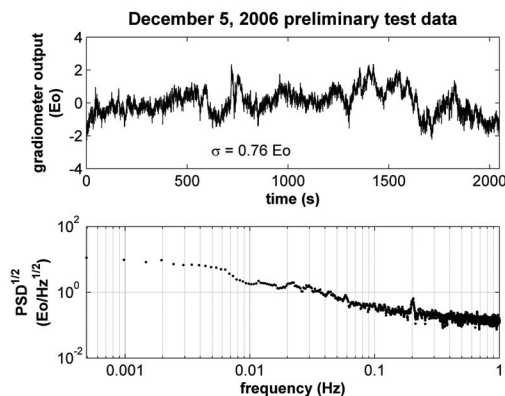


Figure 3: Dec. 5, 2006 laboratory test results.

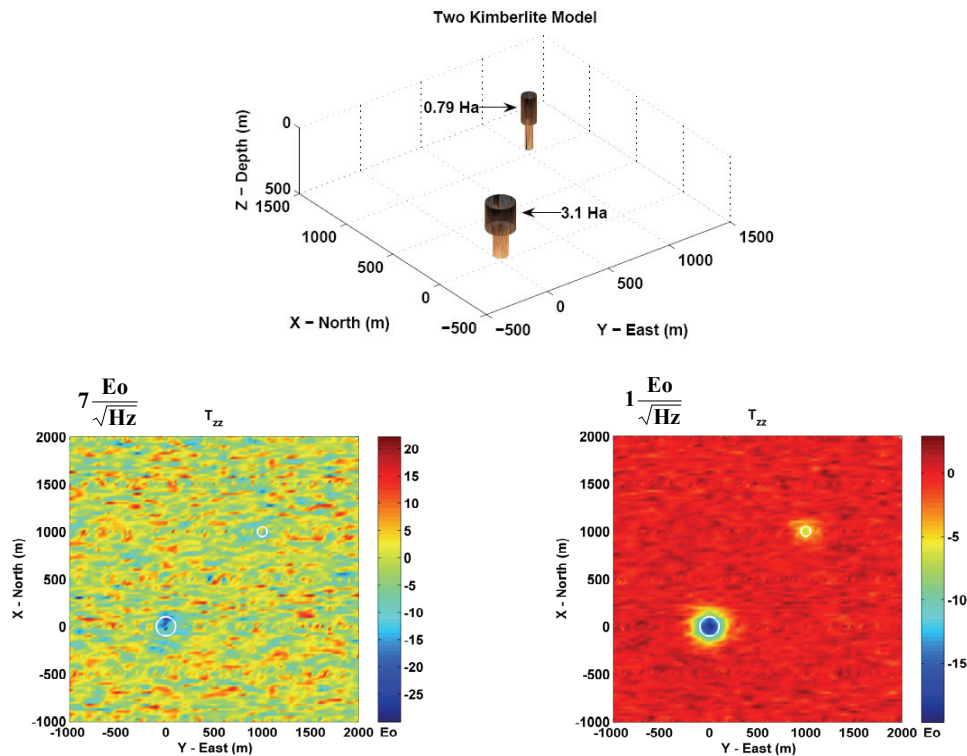


Figure 4: Two-kimberlite model having parameters listed in Table 1 and Γ_{xx} response with $1 \text{ Eo}/\sqrt{\text{Hz}}$ noise and $7 \text{ Eo}/\sqrt{\text{Hz}}$ noise, from 0.001 Hz to 1 Hz, added. An aircraft speed of 100 knots is assumed.

CONCLUSION

A superconducting gravity gradiometer on a platform which isolates the gradiometer from high frequency motion is required to achieve a target noise level of $1 \text{ Eo}/\sqrt{\text{Hz}}$ from 0.001 Hz to 1 Hz, or over wavelengths of tens of meters to tens of kilometers assuming an aircraft speed of 100 knots. This target performance will provide improvements in the airborne detection and imaging of natural resources of economic interest.

ACKNOWLEDGMENTS

Thank you to Natural Resources Canada for the information provided about kimberlite exploration in Canada on the following website:

http://atlas.nrcan.gc.ca/site/english/maps/economic/diamond_exploration/locationofkimberlites.

REFERENCES

- Boggs, D. B., Lee, J. B., Maddever, R. A. M., van Leeuwen, E. H., Turner, R. J., Downey, M. A., McCracken, K. G. and Liu, G., 2005, The BHP Billiton digital gravity gradiometer: Preview, **117**, 21-22.
- Boggs, D. B., Maddever, R. A. M., Lee, J. B., Turner, R. J., Downey, M. A., and Dransfield, M. H., 2007, First test survey results from the Falcon helicopter-borne airborne gravity gradiometer system: Preview, **126**, 26-28.
- Gravity and Magnetics Research Consortium, 2003, Report: A program library for forward modeling and inversion of gravity gradient data over 3D structures GG3D Version 1.0, Department of Geophysics, Colorado School of Mines, Golden, Colorado.
- Li, X., 2001, Vertical resolution: Gravity versus vertical gravity gradient: The Leading Edge, **20**, 8, 901-904
- Mickus, K. L. and Hinojosa, J. H., 2001, The complete gravity gradient tensor derived from the vertical component of gravity: a Fourier transform technique, Journal of Applied Geophysics, **46**, 159-174.
- Moody, M. V. and Paik, H. J., 2004, A Superconducting Gravity Gradiometer for inertial navigation: Position Location and Navigation Symposium April 26-29, 2004: PLANS 2004, 775 – 781.

Murphy, C. A., Brewster, J., and Robinson, J., 2007, Evaluating Air-FTG survey data: Bringing value to the full picture: Preview, **126**, 24-25, 28.